*Sensors* **2013**, *13*, 4428-4449; doi:10.3390/s130404428

OPEN ACCESS

*sensors*

**ISSN 1424-8220**

www.mdpi.com/journal/sensors

*Article*

# Dosimeter-Type $NO_x$ Sensing Properties of $KMnO_4$ and Its Electrical Conductivity during Temperature Programmed Desorption

**Andrea Groß [1], Michael Kremling [1], Isabella Marr [1], David J. Kubinski [2], Jacobus H. Visser [2], Harry L. Tuller [3] and Ralf Moos [1,*]**

[1] Zentrum für Energietechnik, Bayreuth Engine Research Center (BERC), Department of Functional Materials, University of Bayreuth, 95440 Bayreuth, Germany; E-Mails: andrea.gross@uni-bayreuth.de (A.G.); m.kremling@googlemail.com (M.K); isabella.marr@uni-bayreuth.de (I.M.)

[2] Ford Research and Advanced Engineering, Dearborn, MI 48124, USA; E-Mail: dkubinsk@ford.com

[3] Department of Materials Science and Engineering, Massachusetts Institute of Technology, Cambridge, MA 02139, USA; E-Mail: tuller@mit.edu

* Author to whom correspondence should be addressed; E-Mail: Functional.Materials@Uni-Bayreuth.de; Tel.: +49-921-55-7401; Fax: +49-921-55-7405.

*Received: 28 February 2013; in revised form: 22 March 2013 / Accepted: 25 March 2013 / Published: 2 April 2013*

---

**Abstract:** An impedimetric $NO_x$ dosimeter based on the $NO_x$ sorption material $KMnO_4$ is proposed. In addition to its application as a low level $NO_x$ dosimeter, $KMnO_4$ shows potential as a precious metal free lean $NO_x$ trap material (LNT) for $NO_x$ storage catalysts (NSC) enabling electrical *in-situ* diagnostics. With this dosimeter, low levels of NO and $NO_2$ exposure can be detected electrically as instantaneous values at 380 °C by progressive $NO_x$ accumulation in the $KMnO_4$ based sensitive layer. The linear $NO_x$ sensing characteristics are recovered periodically by heating to 650 °C or switching to rich atmospheres. Further insight into the $NO_x$ sorption-dependent conductivity of the $KMnO_4$-based material is obtained by the novel eTPD method that combines electrical characterization with classical temperature programmed desorption (TPD). The $NO_x$ loading amount increases proportionally to the $NO_x$ exposure time at sorption temperature. The cumulated $NO_x$ exposure, as well as the corresponding $NO_x$ loading state, can be detected linearly by electrical means in two modes: (1) time-continuously during the sorption interval including $NO_x$ concentration information from the signal derivative or (2) during the short-term thermal $NO_x$ release.

**Keywords:** $NO_x$ dosimeter; lean $NO_x$ trap (LNT); precious metal free $NO_x$ storage catalyst (NSC); electrical TPD; accumulating sensing principle; low ppm-level $NO_x$ detection; *in-situ* catalyst loading state monitoring; ammonia SCR; three-way catalyst (TWC)

## 1. Introduction

Highly sensitive, selective, stable and fast responding $NO_x$ sensing devices are required for the reliable detection of low levels of $NO_x$ in a number of important application areas, including automotive and industrial emissions control, as well as environmental and air quality monitoring (immission) [1–3]. Often, the main requirement is the ability to monitor $NO_x$ mean concentration values over extended periods (e.g., 1-hour value for immission legislation [4], or the emitted concentration per driven distance [5]) instead of the instantaneous concentration. Dosimeter, integrating or accumulating-type sensors, largely operated as optical or mass sensitive devices, are designed to meet these requirements. Analyte accumulation affects the sensor signal and is achieved either by the generation of a reaction product with the sensor active layer [6–11], or irreversible sorption of $NO_x$ onto the surface layer [12–14], followed by periodic regeneration of the sorption capacity [12,14–17].

Recently, impedimetric or resistive $NO_x$ dosimeters, based on materials utilized in automotive lean $NO_x$ trap catalysts (LNT), were successfully introduced [6,11,18]. Around 400 °C, these carbonate-based materials enable long-term detection of low levels of NO and $NO_2$ by monitoring the increase in conductivity with increased $NO_x$ loading. The zero-level is reset by regeneration, achieved either by a step change in temperature or by exposure to reducing atmospheres [6].

In this study, $KMnO_4$ is investigated as a low-cost alternative to commercial LNT formulations in a dosimeter-type $NO_x$ sensing device. $KMnO_4$ is known as a strong oxidant [19–21], forming nitrites and nitrates upon exposure to $NO_x$, even above the $KMnO_4$ decomposition temperature [22,23]. Following an investigation of its electrical properties, the $NO_x$ dosimeter-type sensing properties at elevated temperatures and the effect of periodic thermal regeneration are examined. The $NO_x$ dose is measured either during sorption or during regeneration by combining the conventional temperature programmed desorption method with the electrical sensor signal. This technique, denoted as eTPD, provides, for the first time, a quantitative correlation between the electrical properties and the $NO_x$ loading state of a material. This should be of interest for both sensing and catalyst diagnosis applications.

## 2. $KMnO_4$/La-$Al_2O_3$ as Sensitive Layer

### *2.1. Sample Preparation and Characterization*

The sensitive layer of the proposed $NO_x$ dosimeter was prepared from 17 mol% $KMnO_4$ (Merck) deposited onto alumina, stabilized with 3% lanthanum (Puralox SCFa-140La3), serving as support oxide with surface area of 140 $m^2/g$ and mean particle diameter of 30 µm. The $KMnO_4$/La-$Al_2O_3$ powder was prepared by multiple infiltration of an aqueous solution of $KMnO_4$ into the La-$Al_2O_3$ powder, followed by drying at 100 °C and calcination at 600 °C for 5 h. Upon thermal decomposition $KMnO_4$ is known to form various potassium- and manganese-containing compounds, like $K_2MnO_4$

and $K_3MnO_4$, as well as manganese oxide $MnO_x$ existing in different oxidation states [22,24–30]. The decomposition of $KMnO_4$ is reported by Boldyrev [25,26] to become noticeable in the temperature range from 205 to 280 °C. $KMnO_4$-impregnation and firing decreased the surface area of the powder to 100 $m^2/g$ (obtained by BET method (named after the originators of the method: Brunauer, Emmett, and Teller) relying on the adsorption of gases to determine the specific surface area of powders). The SEM (scanning electron microscope) analysis of the fired $KMnO_4/La\text{-}Al_2O_3$ powder is given in Figure 1 as a backscatter electron (BSE) image. The powder consists of spherical $La\text{-}Al_2O_3$-rich particles in the range of some tens of µm, partly embedded in a potassium and manganese comprising matrix, which was confirmed by energy-dispersive X-ray spectroscopy (EDX) measurements.

**Figure 1.** SEM image (BSE) of $KMnO_4/La\text{-}Al_2O_3$ powder after firing. The Al-rich particles and the K-Mn-rich matrix are indicated.

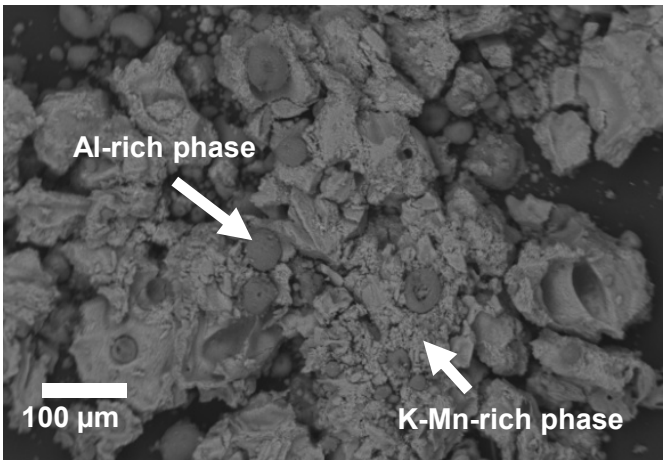


The $KMnO_4/La\text{-}Al_2O_3$ powder was mixed with an organic binder (KD2721, Zschimmer & Schwarz) in order to obtain a processable paste. The paste was deposited by spatula onto a 96% pure alumina substrate equipped with gold interdigitated electrodes (area 5 × 6 mm, finger width/distance 100 µm) and fired at 600 °C. The sample was pre-conditioned for several hours at temperatures up to 650 °C in $NO_x$ containing oxygen-rich atmospheres.

**Figure 2.** Sensor setup and test apparatus including the gas dosing system, a quartz tube furnace containing the $KMnO_4/La\text{-}Al_2O_3$ sample and a chemiluminescence detector (CLD, 700 EL ht, Ecophysics).

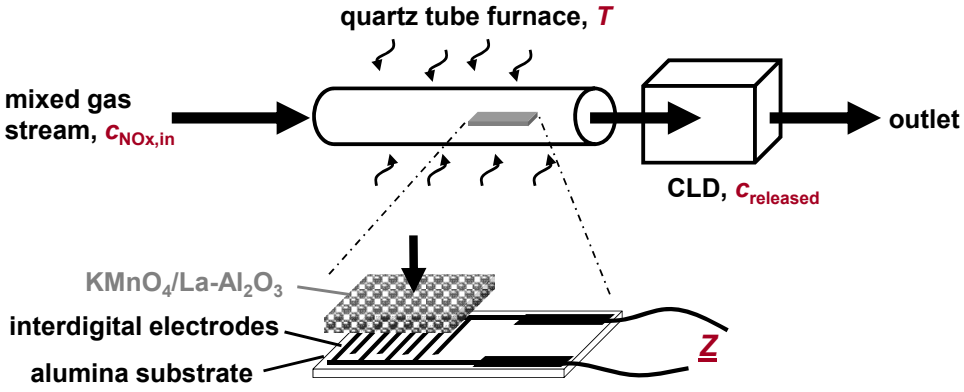

The electrical properties of $KMnO_4$/La-$Al_2O_3$ were investigated in a test apparatus as sketched in Figure 2. Following installation in a quartz-tube furnace with inner diameter of 22 mm, the sample was heated to temperatures between 300 to 650 °C. The $KMnO_4$/La-$Al_2O_3$ layer was exposed to a 2 L/min lean gas flow (10% $O_2$, 50% $N_2$ humidified with a water bubbler at room temperature, and 5% $CO_2$ diluted in $N_2$ balance) with a gas exchange time of the system in the range of 8 s. The impedance $\underline{Z}$ of the $KMnO_4$/La-$Al_2O_3$ sample was recorded by an impedance analyzer (Alpha High Performance Frequency Analyzer, Novocontrol).

### *2.2. Electrical Properties in the Unloaded State*

The electrical properties of $KMnO_4$/La-$Al_2O_3$ in the unloaded state (after regeneration of the $NO_x$ sorption sites) were evaluated from 300 to 650 °C by impedance spectroscopy in the frequency range of 1 Hz to 1 MHz. Plotting the impedances in the complex plane as Nyquist plots (real part *Z'* and imaginary part *Z''*) yields near semicircular spectra at higher frequencies. This allows the bulk impedance to be modeled by a resistance *R* in parallel to a constant phase element *CPE* (*R*||*CPE*). The corresponding impedance $\underline{Z}_{CPE}$ expressed as a function of the model parameters *n* (ranging from 0 to 1) and *Q* as well as the angular frequency $\omega$ is given in Equation (1):

$$\underline{Z}_{CPE}(\omega) = \frac{1}{Q}(i\omega)^{-n} \quad (1)$$

In Figure 3(a and b), examples for the corresponding Nyquist plots of the measured impedance data (dots) for 380 and 650 °C, together with the fitted *R*||*CPE* curves in the upper frequency range (solid curves) and the corresponding fitting parameters, are displayed. While the $KMnO_4$/La-$Al_2O_3$ sample has a resistance of 180 kΩ at 380 °C, it decreases to 3.4 kΩ upon heating to 650 °C.

The electrical conductivity σ of the $KMnO_4$/La-$Al_2O_3$ specimen was estimated from the fitted *R*-values of the impedance in the *R*||*C* dominated frequency range taking into account the electrode geometry. The electrode geometry is estimated from the capacitance of the uncoated structure, assuming a parallel-plate capacitor, as described in [31]. The resulting Arrhenius-like representation of σ as a function of inverse temperature 1/*T* in Figure 3(c) gives a thermal activation energy of the conductivity $E_A$ of 0.8 ± 0.1 eV. This thermally activated conductivity leads to an almost two decades increase from ~$5 \cdot 10^{-7}$ S/cm at 380 °C to $3 \cdot 10^{-5}$ S/cm at 650 °C.

Information regarding the electrical conductivity of $KMnO_4$-based materials above the decomposition temperature in the literature is limited. In thermoelectric tests, $KMnO_4$ and its decomposition products were identified as *n*-type semiconductors by Boldyrev and Kabanov, and in the literature cited therein [26,28]. Upon thermal decomposition, the conductivity of $KMnO_4$ was found to increase, and depending on morphology, the conductivity was reported to range from $10^{-6}$ to $10^{-8}$ S/cm at 170 to 210 °C [26,28].

The lower conductivity of the $KMnO_4$/La-$Al_2O_3$ based material under investigation compared to the reported conductivity of pure $KMnO_4$ is attributed to the less conductive La-$Al_2O_3$ particles serving as support oxide in the applied sensitive coating. Recently published results on the $K_2CO_3$/La-$Al_2O_3$ system indicate a significant contribution of La-$Al_2O_3$ to the measured conductivity given its lower conductivity than that of pure $K_2CO_3$ [32].

**Figure 3.** Thermal activated conductivity of $KMnO_4$/La-$Al_2O_3$: (**a**) Nyquist plot of the impedance $\underline{Z}$ at 380 and 650 °C, (**b**) enlargement of 650 °C data, (**c**) Arrhenius-like representation of conductivity σ from 300 to 650 °C. Further time-continuous impedance measurements were conducted at 10 kHz (see Section 3.1) and the 10 kHz data points in (**a**) and (**b**) are highlighted.

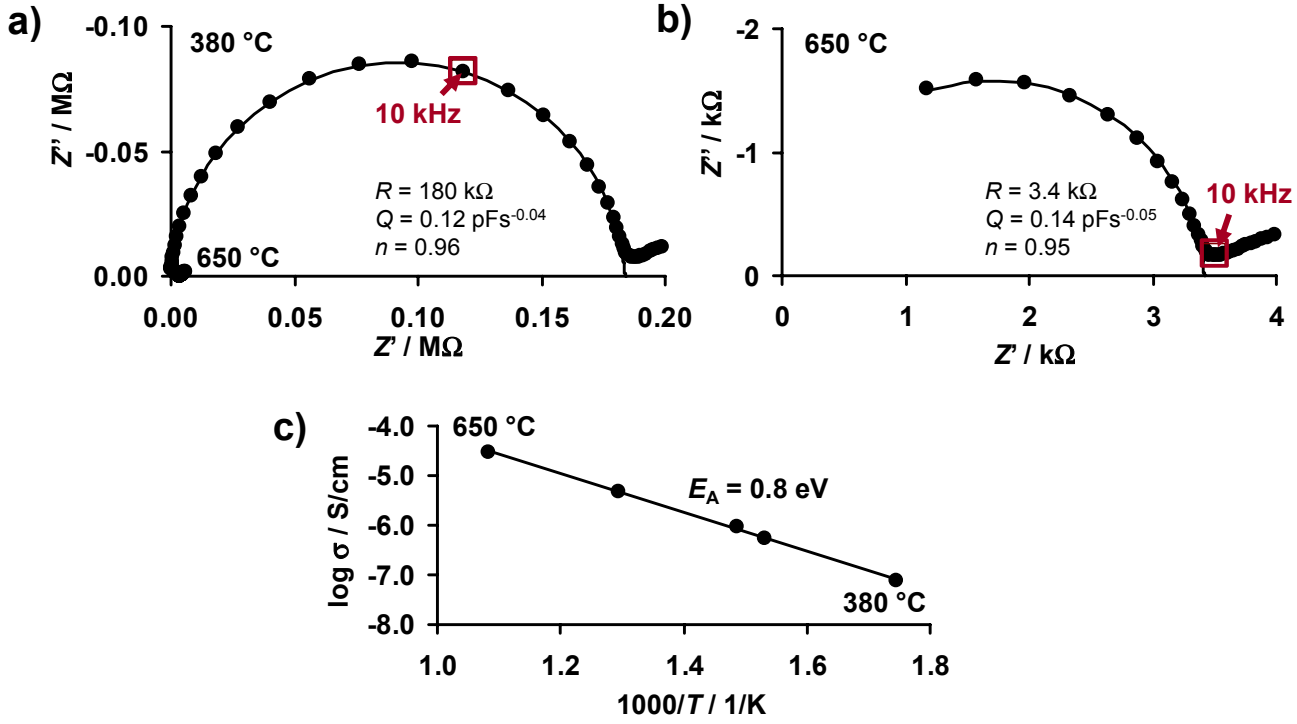


## 3. $NO_x$ Sensing Properties

Similar to passive samplers, dosimeter-type gas sensors are operated in two alternating steps: Analyte molecules are progressively accumulated in the sensitive layer during a sorption period, followed by a regeneration procedure to release the formerly sorbed molecules. The focus of the next section is on the evaluation of the dosimeter-type $NO_x$ sensing characteristics of $KMnO_4$/La-$Al_2O_3$ during $NO_x$ sorption as well as the efficiency of thermal regeneration.

### *3.1. Experimental Setup and Data Evaluation*

To study the effect of $NO_x$ in the low ppm range, the $KMnO_4$/La-$Al_2O_3$ sample was exposed to various NO and $NO_2$ concentrations, $c_{NO,in}$ and $c_{NO_2,in}$ for defined time intervals $t_{NOx,in}$. $NO_x$ was admixed to the 2 L/min lean base gas flow (10% $O_2$, 50% $N_2$ humidified with a water bubbler at room temperature, and 5% $CO_2$ diluted in $N_2$ balance). The outlet concentrations were determined by a chemiluminescence detector, as illustrated in Figure 2. In accordance to the reported catalytic activity of Mn-containing LNTs [23,33–36], as well as to results on LNT-based $NO_x$ dosimeters [6,18], the $NO_x$ sorption studies were performed at a sorption temperature $T_{sorption}$ of 380 °C, with periodic heating to 650 °C for regeneration.

The sample impedance was recorded continuously during $NO_x$ exposure. Since the fitted *n*-parameters of $\underline{Z}_{CPE}$ (Equation (1)) of $KMnO_4$/La-$Al_2O_3$ in the high frequency range were found to be

close to 1 (≈0.95), $Q$ can be approximated by the capacitance $C$ and the $R||CPE$ equivalent circuit model can be simplified to an $R||C$ circuit. Thus, $R$ is calculated from the absolute value of the impedance $|\underline{Z}|$ and the phase angle $\varphi$ at a fixed frequency according to Equation (2).

From the Nyquist plots in Figure 3, 10 kHz (marked in red) was selected as an appropriate measurement frequency to monitor the temperature dependent electrical properties in the $R||C$ dominated range over time and was used, if not denoted otherwise. The absolute value of the relative resistance change due to $NO_x$ exposure $\Delta R_{rel}$ is denoted as the sensor signal, and is defined by Equation (3), with $R_0$ being the base resistance in the $NO_x$ unloaded state:

$$R = |Z| \cdot \sqrt{1 + \tan^2 \varphi} \tag{2}$$

$$\Delta R_{rel} = \frac{|\Delta R|}{R_0} = \frac{R_0 - R}{R_0} \tag{3}$$

The analysis in terms of dosimeter-type sensing properties during $NO_x$ sorption at constant flow rates is illustrated in Figure 4. During the $NO_x$ loading stage, $\Delta R_{rel}$ is expected to increase in the presence of $NO_x$ at $T_{sorption}$ due to progressive $NO_x$ accumulation, without recovery (Figure 4(a)). In the case of a constant flow rate, the cumulated $NO_x$ exposure (or dose) $A_{NOx,in}$ is given by the time integral of $c_{NOx,in}$ as sketched in Figure 4(b), resulting in the unit ppm·s [6,16,37].

**Figure 4.** Data analysis during progressive $NO_x$ accumulation at $T_{sorption}$: (**a**) increase in sensor response $\Delta R_{rel}$ during $NO_x$ sorption, (**b**) determination of cumulated $NO_x$ exposure $A_{NOx,in}$, (**c**) characteristic $\Delta R_{rel}$ *vs.* $A_{NOx,in}$ line.

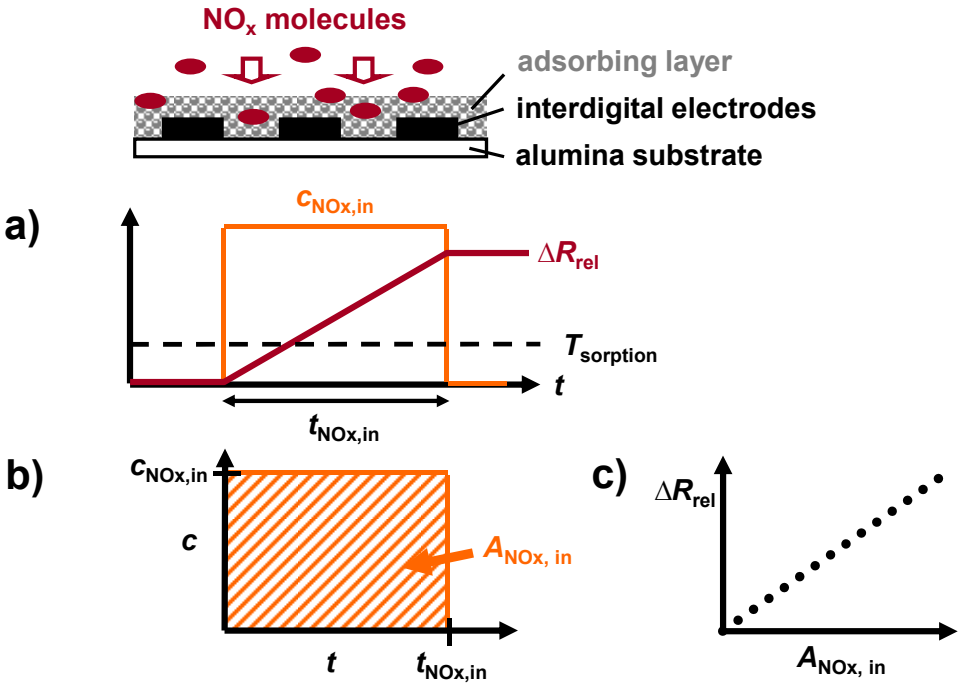


At a constant $NO_x$ concentration, $A_{NOx,in}$ scales linearly with $t_{NOx,in}$. The resulting characteristic line in Figure 4(c) correlates $\Delta R_{rel}$ with $A_{NOx,in}$. It has been shown in detail for a similar material in [6] that in the case of a linear correlation, the signal derivative of a $NO_x$ dosimeter at a constant flow rate increases with the actual $NO_x$ concentration.

### *3.2. Cumulative $NO_x$ Detection at 380 °C*

The presence of $NO_x$ was found to decrease the resistivity of $KMnO_4$/La-$Al_2O_3$, with the electrical response continuing to satisfy the $R||C$ equivalent circuit (not shown). The temporal dependence of $R$ on $NO_x$ at 380 °C was studied by exposing the sample to pulses of NO and $NO_2$ for periods of $t_{NOx,in}$ = 100 s with concentrations ranging up to 16 ppm. The pulse heights in terms of $c_{NO,in}$ and $c_{NO2,in}$, together with the resulting sensor response, are displayed in Figure 5(a). The sensor response $\Delta R_{rel}$ (Equation (3)) increases stepwise in the presence of NO and $NO_2$ without any recovery at 0 ppm $NO_x$. The slope of $\Delta R_{rel}$ *vs.* $t$ increases with $c_{NOx,in}$. The characteristic line in Figure 5(b) is extracted from the measured data points and the course of the $NO_x$ concentration according to Figure 4. $\Delta R_{rel}$ correlates almost linearly with the cumulated $NO_x$ exposure $A_{NOx,in}$, independent of the $NO_x$ species, up to at least 40% signal change with a $NO_x$ sensitivity of 4.8%/1,000 ppm·s. The specimen thus provides comparable sensitivity to both NO and $NO_2$. Small deviations of the $NO_2$ related data points from linearity at the initial stage of exposure may originate from $NO_2$ adsorption on the inner surface of the feed lines. The sensing characteristics and in particularly the sensitivity of $NO_x$ dosimeter with a comparable sensitive material were found to be dependent on the temperature as well as on the thickness of the sensitive layer [6,16].

**Figure 5.** $NO_x$ sensing properties at 380 °C (10% $O_2$, 50% $N_2/H_2O$, 5% $CO_2$ in $N_2$): (**a**) stepwise increase of sensor response $\Delta R_{rel}$ (Equation (3)) during cyclic exposure to NO or $NO_2$, (**b**) resulting linear $\Delta R_{rel}$ *vs.* $A_{NOx,in}$ characteristic line.

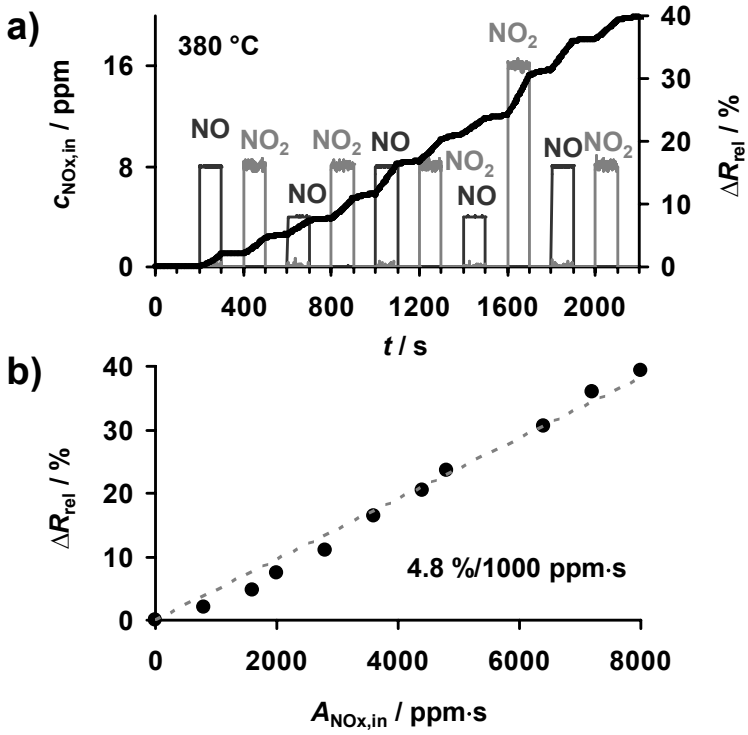


Figure 5 indicates the strong and progressive sorption of NO and $NO_2$ onto $KMnO_4$/La-$Al_2O_3$ at 380 °C with corresponding impact on its electrical conductivity. As in K-Mn-containing LNTs [21,23], $NO_x$ is expected accumulate on $KMnO_4$/La-$Al_2O_3$ by forming stable nitrates on the potassium sites generated upon $KMnO_4$ decomposition [22]. For LNTs it is well known that NO is first oxidized to

$NO_2$ on redox active sites provided by e.g., precious metals, followed by chemical $NO_2$ storage by reaction with the alkaline (earth-) carbonates, mainly $BaCO_3$ or $K_2CO_3$, to form nitrates [38–40]. The observed increase in the conductivity of fully formulated LNTs in $NO_x$ enables their application as total $NO_x$ sensors [6,11,41] or for *in-situ* diagnostics of automotive catalysts [41–43].

The requirement of an incorporated oxidant, for the purpose of NO sorption, was verified by electrical means. Pure $BaCO_3$ or $K_2CO_3$, on the other hand, accumulates only $NO_2$, enabling conductometric $NO_2$ dosimetry, without NO cross-sensitivity [15,32]. Given the ability of $KMnO_4$/La-$Al_2O_3$ to detect either NO or $NO_2$, the oxidizing properties of $KMnO_4$/La-$Al_2O_3$ are demonstrated to be sufficient to convert NO to $NO_2$ prior to nitrate formation. This is consistent with $MnO_x$, as a product of $KMnO_4$ decomposition [25,27], being known as an effective oxidizing agent in $NO_x$ reduction catalysts [22,24,33,34,36,44]. The contribution of $MnO_x$ to the $NO_x$ sorption capacity at 380 °C cannot be excluded [45–48].

The linear correlation between $\Delta R_{rel}$ and $A_{NOx,in}$ in the low loading state of the $NO_x$ dosimeter based on $KMnO_4$/La-$Al_2O_3$ in Figure 5 points on a sorption rate proportional to the $NO_x$ concentration. This linearity provides a dual-mode functionality: while the sensor response corresponds directly to the cumulated $NO_x$ exposure during the sorption period, the course of $c_{NOx,in}$ can be determined via the signal derivative as described in [6,14]. Furthermore, these results demonstrate that decomposed $KMnO_4$ can be utilized in $NO_x$ dosimeters and catalysts *without* any need for expensive precious metal additives due to its intrinsic oxidizing nature.

### *3.3. $NO_x$ Concentration Sensitivity at 650 °C*

An important criterion for a useful sensor is the ability to refresh or regenerate the device following accumulation of the target gas analyte, which in this study is $NO_x$. The decreased thermodynamic stability of the formed nitrates upon heating limits the catalytic activity of LNTs [38–40,49] and alters the cumulative $NO_x$ sensing characteristics of carbonates and LNT-based sensors [6,17,18,32]. According to Becerra *et al.* [22], nitrate and nitrite-like compounds formed on $KMnO_4$-based materials decompose in the temperature range of ~550 to 670 °C. Hence, a thermal release of sorbed $NO_x$, leading to a recovery of the sorption sites of $KMnO_4$/La-$Al_2O_3$, seems feasible.

The effect of $NO_x$ on the resistivity of $KMnO_4$/La-$Al_2O_3$ was studied at 650 °C to investigate this temperature as being suitable for regeneration. The sample was exposed to the $NO_x$ concentration profile shown in Figure 6(a) with up to 8 ppm NO and 75 ppm $NO_2$. $\Delta R_{rel}$ is calculated from the impedance at 1 MHz due to the increased conductivity. Again, the conductivity of $KMnO_4$/La-$Al_2O_3$ increases in the presence of $NO_x$. But, as shown in Figure 6(b), at 650 °C, the value for $\Delta R_{rel}$ follows the course of $c_{NOx,in}$ (instead of $\int c_{NOx,in}\, dt$) being characteristic of a common concentration-detecting gas sensor response. Despite the corresponding concentration-related characteristic line in Figure 6(c), which gives a linear correlation, the low sensitivity of only 2.7%/100 ppm $NO_2$ limits the application of $KMnO_4$/La-$Al_2O_3$ as a $NO_x$ sensing material operated at 650 °C.

The reversibly sensor response at 650 °C in Figure 6 indicates that the equilibrium of the $NO_x$ sorption on the $KMnO_4$-based material is shifted to the side of the reactants and the resulting fast desorption goes along with the loss of $NO_x$ accumulation capability. Hence, 650 °C seems an appropriate temperature to release formerly sorbed $NO_x$ and to recover the sorption capacity, as well as

the electrical properties of $KMnO_4/La\text{-}Al_2O_3$. The reversibility of the sensor response of $KMnO_4/La\text{-}Al_2O_3$ at 650 °C is consistent with results on an LNT-based $NO_x$ dosimeter [17].

**Figure 6.** $NO_x$ concentration detection at 650 °C: (**a**) course of $NO_x$ concentration $c_{NOx,in}$, (**b**) sensor response $\Delta R_{rel}$, (**c**) linear correlation between $\Delta R_{rel}$ and $c_{NOx,in}$.

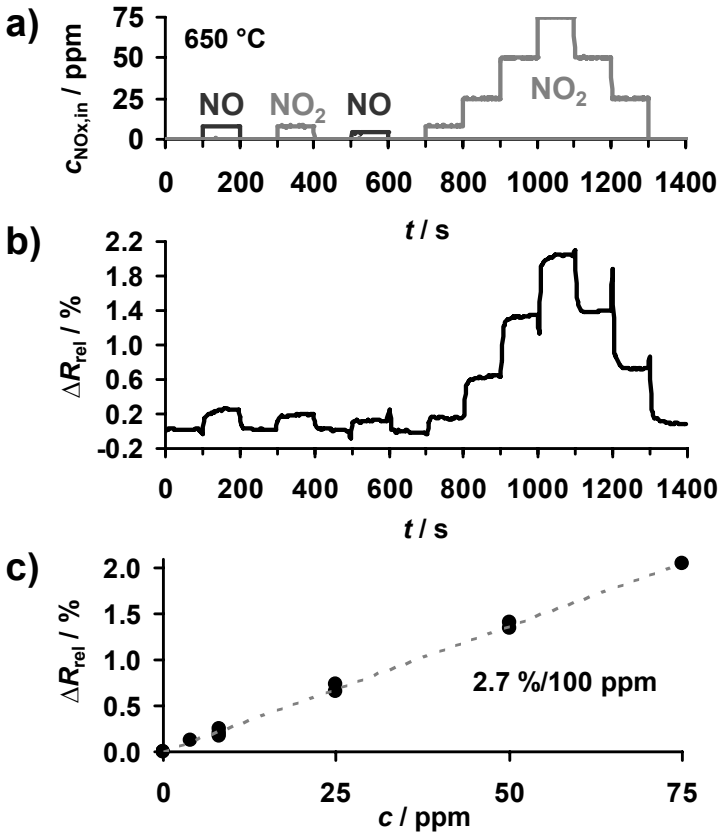


*3.4. Efficiency of Thermal Regeneration*

In the following test series, the efficiency of thermal regeneration, the reproducibility of the dosimeter-type $NO_x$ sensing characteristics, and the influence of $NO_x$ exposure time were studied. The same $KMnO_4/La\text{-}Al_2O_3$ sample was exposed to 8 ppm $NO_2$ or NO at 380 °C in periods of 250, 500, 750, 1,000, and 2,000 s. Between each $NO_x$ exposure period, the sample was regenerated at 650 °C for about 5 min in the lean gas flow. The sensor responses as a function of $t_{NO_2,in}$ and $t_{NO,in}$ are compared in Figure 7. The five $NO_2$-borne curves of $\Delta R_{rel}$ depicted in Figure 7(a) are almost identical in the corresponding overlapping time scales; please note that the data points corresponding to the longest $NO_2$ exposure of 2,000 s are partly masked by the other data curves. The corresponding NO curves up to 1,000 s in Figure 7(b) are overlapping as well. The sensor behaves linearly (following an initial incubation period) up to a resistance change of about 40%, with the slope of $\Delta R_{rel}$ in Figure 7(a) being nearly constant up to about 1,000 s (8,000 ppm·s $NO_2$). The nonlinearity at the beginning of $NO_x$ exposure in Figures 5 and 7, *i.e.*, the slight initial slope increase during the first 375 s in $NO_2$ (3,000 ppm·s $NO_2$), is assumed to be caused by $NO_x$ (in particular $NO_2$) being adsorbed on the feed gas lines resulting in a delayed sensor response. Further $NO_2$ exposure leads to a decrease in the slope and $\Delta R_{rel}$ reaches a value of 70% after half an hour in 8 ppm $NO_2$. By definition, $\Delta R_{rel}$ cannot reach 100%

as the conductivity increases, resulting in a flattening of the curve of $\Delta R_{rel}$ with continuing $NO_x$ loading. It is expected that a greater sensitive layer thickness would increase the linear range to higher $NO_x$ levels, but at reduced sensitivity (slope $d(\Delta R_{rel})/dA_{NOx,in}$), as reported for LNT-based dosimeters [16].

**Figure 7.** Repeated sensor response to 8 ppm $NO_x$ intervals with intermediate regeneration: (**a**) sensor response $\Delta R_{rel}$ during $NO_2$ for $NO_2$ exposure of $t_{NO_2,in}$ as indicated, (**b**) $\Delta R_{rel}$ during NO for $t_{NO,in}$ as indicated.

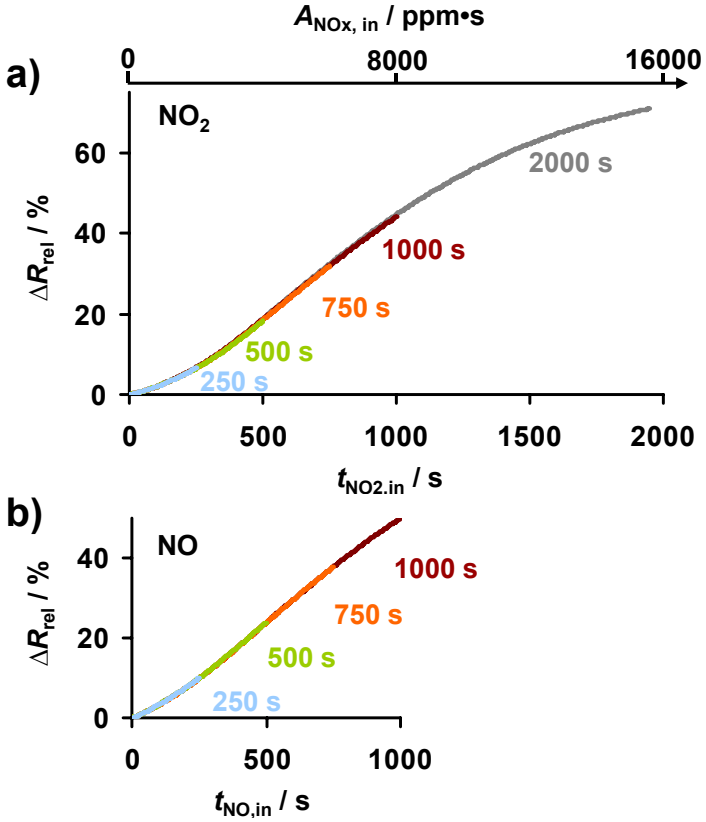


The reproducibility of the sensor response in Figure 7 indicates that the sorption sites of the $KMnO_4/La\text{-}Al_2O_3$-based dosimeter material can be recovered by releasing sorbed $NO_x$ thermally. Heating up to 650 °C restores the $NO_x$ sensing characteristics at 380 °C, independent of the former $NO_x$ exposure duration. The base resistance in the unloaded state $R_0$ was found to decrease slightly with time without impacting the $NO_x$ sensitivity. This might be attributed to small morphological changes during thermal aging, which, however, are too small to be seen by SEM. It is noteworthy to mention that the dosimeter principle avoids such long term signal drifts by definition, since the zero level of $\Delta R_{rel}$ is reset after each regeneration step. This is one of the key advantages of conductometric dosimeters compared to classical semiconductor gas sensors.

## 4. Electrical Conductivity during Temperature Programmed Desorption (eTPD)

As in temperature programmed desorption (TPD) studies, the course of the $NO_x$ concentration due to $NO_x$ desorption during thermal regeneration gives quantitative information about the amount of stored $NO_x$ in $KMnO_4/La\text{-}Al_2O_3$. Combining TPD with simultaneous electrical characterization (eTPD), an electrical readout of the cumulative sorbed $NO_x$ during the short thermal regeneration periods

results. To obtain further insight into the relation between the $NO_x$ loading state and the electrical behavior during $NO_x$ sorption and release, eTPD is applied to the $KMnO_4/La\text{-}Al_2O_3$ formulation.

### *4.1. eTPD Setup and Data Evaluation*

eTPD on $KMnO_4/La\text{-}Al_2O_3$ is performed with the experimental arrangement shown in Figure 2. The eTPD related data and their evaluation are summarized in Figure 8.

**Figure 8.** Data analysis for eTPD: (**a**) time dependence of conductance log $G$ and outlet $NO_x$ concentration $c_{released}$, (**b**) determination of released amount $A_{released}$ and electrical response $F_G$, (**c**) $F_G$ as a function of $A_{released}$.

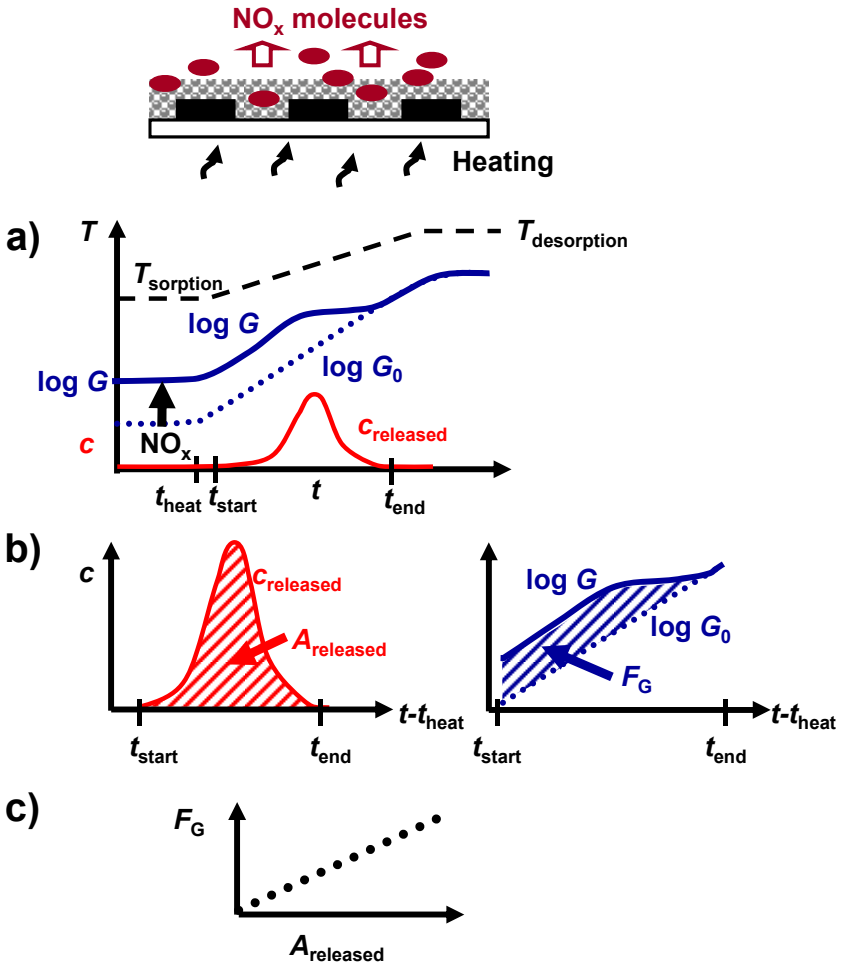


To recover the $NO_x$ sensing characteristics of $KMnO_4/La\text{-}Al_2O_3$ in between the $NO_x$ sorption intervals in the lean gas flow in Figure 7, the sample was heated from 380 °C ($T_{sorption}$) to 650 °C ($T_{desorption}$) with a heating rate of 74 °C/min from 425 to 635 °C, while monitoring the impedance at 10 kHz. The temperature increase started at $t_{heat}$, 50 s after the end of the preceding $NO_x$ dosing interval. The resulting $NO_x$ desorption curve (Figure 8(a)) is displayed as a $NO_x$ concentration $c_{released}$. At $t_{start} = t_{heat} + 50$ s an increase of $NO_x$ is observed in the outlet until $t_{end}$. As illustrated in Figure 8(b), at a constant flow rate, the time integral of $c_{released}$, evaluated in the time interval of $t_{end} - t_{start} = 300$ s, reflects the released $NO_x$ amount $A_{released}$. $A_{released}$ is expected to be proportional to the quantity of sorbed $NO_x$, if the sorption sites are fully recovered by heating.

The conductance $G$ of $KMnO_4$/La-$Al_2O_3$, with $G = 1/R$, was found to be affected by the temperature and the $NO_x$ loading level, both changing during thermal regeneration. As sketched in Figure 8(a), $NO_x$ release results in a convergence of $G$ to $G_0 = 1/R_0$, $G_0$ being the temperature dependent conductance in the unloaded state. The time integral of the conductance upon heating, relative to those of $G_0$, is evaluated as the cumulative electrical response $F_G$. $F_G$ is calculated according to Equation (4) and is shown in Figure 8(b) as the area between the curves corresponding to the two loading states. In the ideal case, $F_G$ would be a measurand for $A_{released}$ (Figure 8(c)) and would depend linearly on the cumulative sorbed $NO_x$ amount.

$$F_G = \int_{t_{start}}^{t_{end}} [\log G(t) - \log G_0(t)] \mathrm{d}t \tag{4}$$

### *4.2. Evaluation of the Released Amount*

In Figure 7, the resistance responses of $KMnO_4$/La-$Al_2O_3$ during an $NO_2$ sorption series at 380 °C with various exposure periods $t_{NO_2,in}$ are reported. The subsequent regeneration by heating to 650 °C to release the formerly sorbed $NO_x$ can be analyzed in terms of TPD. The corresponding outlet $NO_x$ concentrations $c_{released}$ in the lean 2 L/min gas flow, with a resolution of 0.1 ppm given by the CLD, for $t_{NO_2,in}$ up to 1,000 s are compared in Figure 9. After 1,000 s in 8 ppm $NO_2$ (red curve, as indicated in Figure 9), $KMnO_4$/La-$Al_2O_3$ starts to release $NO_x$ at about 400 °C. $c_{released}$ increases with temperature, and at about 550 °C, a maximum is reached at about 1.3 ppm. Shorter $NO_2$ exposure periods, representing a lower amount of $NO_x$ loading, yield lower peak heights of $c_{released}$. At 650 °C, $c_{released}$ reaches zero for all curves, indicating the end of $NO_x$ release. Additionally, both peak maximum and desorption onset are shifted to lower temperatures with increasing $t_{NO_2,in}$. The latter points to a lower stability of the sorbed $NO_x$ with increased $NO_x$ loading. Concerning the low values of $c_{released}$, it should be considered that the evolved $NO_x$ is diluted in the 2 L/min lean gas flow and that the sensitive $KMnO_4$ coating amounts only to an area of about 30 $mm^2$ (5 × 6 mm).

The reproducibility of the dosimeter-type $NO_x$ sensing characteristics at 380 °C (Figure 7) and the missing $NO_x$ accumulation at 650 °C (Figure 6) reveal that the $NO_x$ sorption capacity of $KMnO_4$/La-$Al_2O_3$ can be recovered by heating to 650 °C. Therefore, the quantity of sorbed $NO_2$ on $KMnO_4$/La-$Al_2O_3$ can be estimated from the subsequently thermally released $NO_x$ amount $A_{released}$, being the area under the desorption peak as shown in Figure 8(b). Figure 9(b) reveals that $A_{released}$ and hence the amount of $NO_x$ sorbed in $KMnO_4$/La-$Al_2O_3$ increases almost linearly (with only a small offset) with $NO_2$ exposure, reflected by $t_{NO_2,in}$. Consequently, $NO_2$ is sorbed on $KMnO_4$/La-$Al_2O_3$ with a time constant sorption rate during the 8 ppm $NO_2$ exposure periods. After 1,000 s in 8 ppm $NO_2$, resulting in a cumulated $NO_2$ exposure of 8,000 ppm·s, about 150 ppm·s $NO_x$ are released. This indicates that only about 1.9% of the $NO_2$ in the passing gas flow is sorbed in the $KMnO_4$ based sensitive layer. The gas velocity of 5.3 m/min together the sensitive area length of 6 mm amounts to a residence time of about 70 ms, being comparable to those in catalysts [37]. However, the huge gas volume above the sensitive layer in the 22 mm diameter quartz tube inhibits full $NO_x$ storage in this $NO_x$ dosimeter setup. The small offset of $A_{released}$ in Figure 9(b) amounts to about $A_{offset} \approx 15$ ppm·s. If one divides this value by the integration time of 300 s, one obtains an average concentration of 0.05 ppm $NO_x$. A closer look at Figure 9(a) reveals that this is (roughly) the offset of the $NO_x$

concentration measurement by the CLD with a resolution of 0.1 ppm. As a conclusion, the offset of $A_{released}$ can be attributed to an integration error. The analysis of the corresponding data after NO exposure yield the same qualitative results (data not shown here) but with a smaller offset. Hence, a further explanation might be the partial overlap of $c_{released}$ with the preceding decay of $c_{NO_2,in}$ due to $NO_2$ adsorption in the feed lines.

**Figure 9.** $NO_x$ release during heating to 650 °C after 8 ppm $NO_2$ exposure for 250 s, 500 s, 750 s, and 1,000 s: (**a**) outlet $NO_x$ concentration $c_{released}$, (**b**) area $A_{released}$ below the curve as depicted in Figure 8(b) as a function of $NO_2$ loading time $t_{NO_2,in}$.

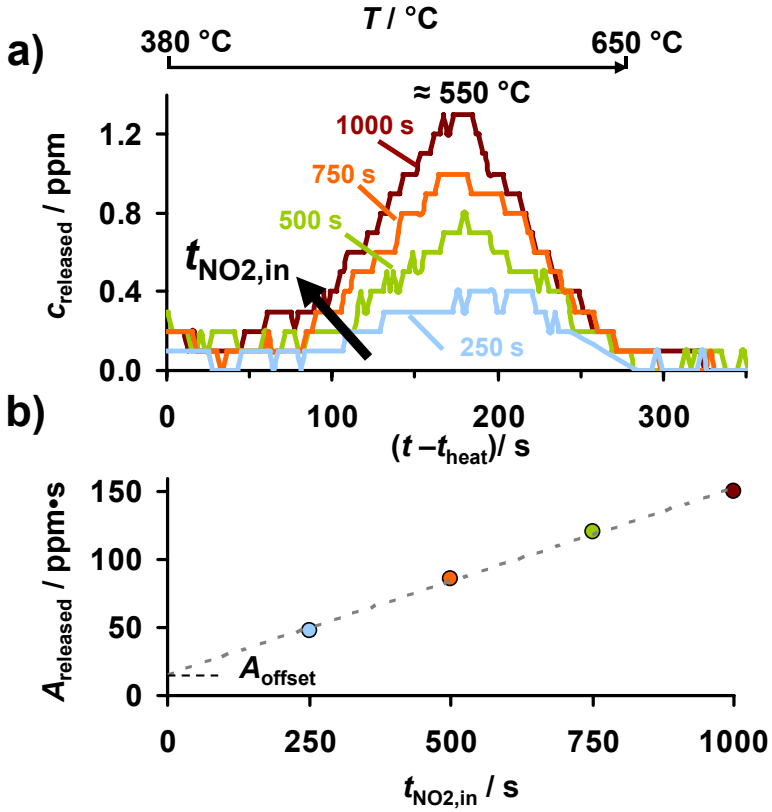


The observed sensor response $\Delta R_{rel}$ of $KMnO_4/La\text{-}Al_2O_3$ during $NO_x$ sorption at 380 °C (Figure 7) obviously corresponds to the amount of loaded $NO_x$. In Figure 10, $\Delta R_{rel}$, caused by 8 ppm NO or $NO_2$ for up to 1,000 s, is related to $A_{released}$, which is obtained from the subsequent regeneration shown in Figure 9. For NO exposure, as well as for $NO_2$ exposure, $\Delta R_{rel}$ increases linearly with $A_{released}$. Hence, in the investigated range, $\Delta R_{rel}$ serves as a linear measure for the NO and $NO_2$ loading levels of $KMnO_4/La\text{-}Al_2O_3$, and due to the constant $NO_x$ sorption rate (Figure 9(b)), also for the cumulated $NO_x$ exposure ($NO_x$ dose). Thereby, the conductivity of $KMnO_4/La\text{-}Al_2O_3$ is slightly more sensitive to NO compared to $NO_2$. From a catalytic point of view, it would be expected that $NO_2$ in the gas flow influences the material's properties more than NO, since $NO_2$ can be sorbed directly as nitrate, whereas NO needs to be oxidized first [23,36]. However, the manganese oxide components of the decomposed $KMnO_4$ might become reduced upon oxidizing NO, thereby affecting the conductivity of $KMnO_4/La\text{-}Al_2O_3$ and hence the NO sensitivity. The delay in the sensor response resulting in an x-axis intercept in Figure 10 is expected to be caused by the already discussed inaccuracy of the determination of $A_{released}$ by integration of small values of evolved $NO_x$ ($A_{Offset} \approx 15$ ppm·s in Figure 9(b)). In addition, $NO_x$

(in particular $NO_2$) adsorption to the feed lines lowers the sensor response but increases the analyzed value for the desorbed amount.

**Figure 10.** Correlation between the sensor response $\Delta R_{rel}$ during NO and $NO_2$ sorption and the $NO_x$ amount $A_{released}$ obtained from subsequent TPD.

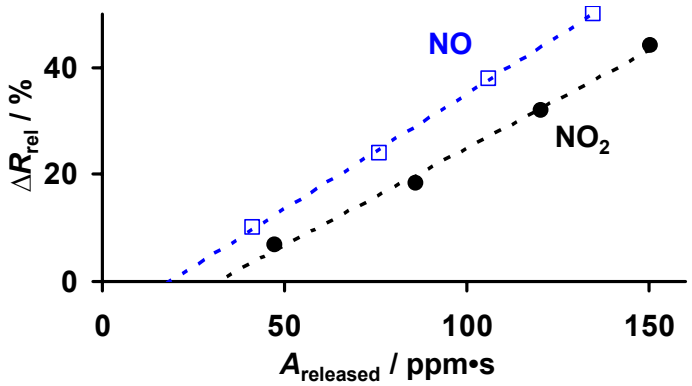


Combining the classical TPD method, with the dosimeter-type electrical response of $KMnO_4$/La-$Al_2O_3$, demonstrates the possibility of sensing $NO_x$ exposure and of electrically monitoring the $NO_x$ loading level of the $NO_x$ sorbent *in-situ*, both with linear correlation at low loading.

### *4.3. Electrical Information upon Thermal Regeneration*

The conductance upon releasing $NO_x$ provides information about the amount of previously sorbed $NO_x$. This may also be useful for $NO_x$ dosimetry. Figure 11a depicts the courses of the conductance $G$ during thermal regeneration after exposure to 8 ppm $NO_2$, for the different loading states indicated by its specific $NO_x$ exposure period $t_{NO_2,in}$. The course of the temperature is shown for comparison (black dots). $G_0$ reflects the conductance in the $NO_x$ unloaded state corresponding to $t_{NO_2,in} = 0$.

Being thermally activated, $G_0$ increases by nearly two orders of magnitude, which agrees with Figure 3. At 380 °C, the conductance in the partly $NO_x$ loaded state $G$ is higher than $G_0$. The difference between $G$ and $G_0$ corresponds to the cumulative $NO_x$ response, $\Delta R_{rel}$ (Figure 7). With progressive temperature, log $G$ increases like log $G_0$. The difference between log $G$ and log $G_0$ increases with $t_{NO_2,in}$, indicating a correlation with the $NO_x$ loading level. Between about 480 and 530 °C, the curves of $G$ start to converge to those of $G_0$. Finally, above about 620 °C (230 s) all curves of $G$ coincide with $G_0$ indicating that the unloaded state is recovered. A more detailed analysis reveals that the inflection point in the course of log $G$ corresponds to the onset of $NO_x$ release shown in Figure 9(a) as $c_{released}$. The temperature of the minimum in the slope of log $G$ coincides with the temperature of the maximum of $c_{released}$. Both are being shifted to lower temperatures, the higher the former loading level was. Hence, the convergence of the curves of log $G$ to the reference in the unloaded state can be attributed to thermal $NO_x$ release from $KMnO_4$/La-$Al_2O_3$, which decreases the temperature-dependent conductivity to the unloaded value.

**Figure 11.** eTPD results after 8 ppm $NO_x$ for up to 1,000 s: (**a**) conductance log *G* and temperature *T* during TPD, (**b**) cumulated electrical response $F_G$ (calculated acc. to Equation (4)) *vs.* the $NO_x$ loading time $t_{NO_2,in}$, (**c**) $F_G$ as a function of the amount of released $NO_x$ $A_{released}$ for NO and $NO_2$ loading, as determined in Figure 9.

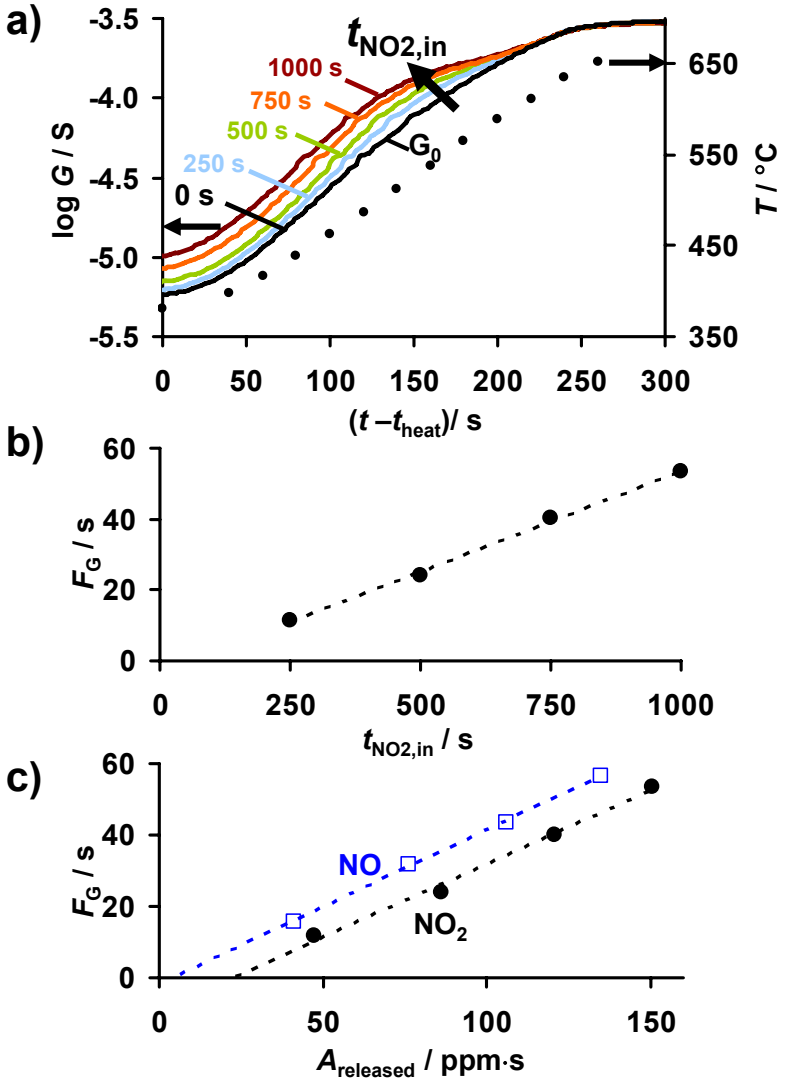


The comparison of the curves of the conductance *G* during regeneration (Figure 11(a)) suggests that the deviation of the course of log *G* from log $G_0$ might reflect the amount of previously sorbed $NO_x$. In fact, Figure 11(b) reveals a linear correlation between $F_G$ calculated according to Equation (4) and the preceding sorption interval $t_{NO_2,in}$. Accounting for the time constant NO and $NO_2$ sorption rate in the low loading state (exemplarily shown for $NO_2$ in Figure 9(b)), $F_G$ is also a linear function of $A_{released}$ as shown in Figure 11(c) for NO and $NO_2$ exposure, respectively. Therefore, besides of $\Delta R_{rel}$, the cumulated electrical response $F_G$ of $KMnO_4$/La-$Al_2O_3$ during regeneration may also be a suitable sensor signal for the cumulated $NO_x$ exposure and the *in-situ* loading level. Again, the resulting sensitivity to NO is slightly higher than those to $NO_2$. Furthermore, the sensor response exhibits an offset, in particular, for $NO_2$. Besides of the small integration error $A_{offset}$ when determining the area under the low level concentration curve during desorption in Figure 9a, these offsets likely originate from $NO_2$ adsorption in the feed lines.

**Figure 12.** Arrhenius-like plot of the eTPD data in different loading states (lines) compared to the equilibrated unloaded state (black dots).

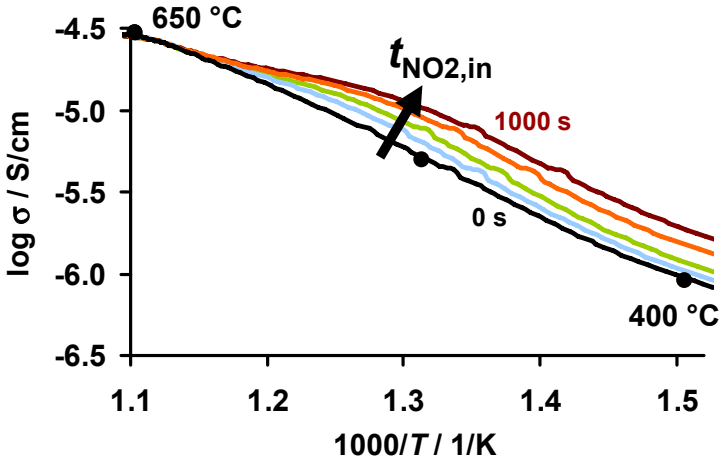


Considering the electrode geometry, the conductivity σ can be calculated from the conductance and the data from Figure 11(a) can be plotted in an Arrhenius-like representation in the area of a constant heating rate as depicted in Figure 12. The data points of the electrical characterization of the $KMnO_4$/La-$Al_2O_3$ sample after equilibration at various temperatures shown in Figure 3(c) are added to Figure 12 as black dots. Concerning the thermally activated conductivity in the unloaded state, the direct comparison reveals that the eTPD data agree well with those obtained in the equilibrated state. This confirms the recovery of the sorption sites by heating to 650 °C. The $NO_x$ saturated state of the carbonates was found to give a more pronounced transition in the curve of the equilibrated temperature-dependent conductivity upon thermal decomposition [32].

The investigation of $NO_x$ sorption on $KMnO_4$/La-$Al_2O_3$ demonstrates that eTPD enables one to correlate the analyte-induced electrical response quantitatively with the actual analyte loading state. This is achieved by observing the electrical properties and the gas desorption characteristics simultaneously. The eTPD method might enhance the understanding of the analyte sorption related electrical properties of functional materials applied for gas sensing or catalysis. Approaches on interpreting the conductivity during thermally releasing gas species are reported in the literature as well, but—to our knowledge—only without a simultaneous quantitative analysis of the desorption peak and hence with a missing correlation with the actual loading state under identical conditions. Colin *et al.* [50] and Fortin *et al.* [51] modeled the electrical influence of chemisorbed gases on semiconductors upon heating and verified it for the system oxygen-CdSe. The slope of the conductivity is reported to give information on desorption or binding energies of the species [51–53]. Rossé *et al.* [53] explains in detail the course of the resistivity in the Arrhenius-like representation during TPD being dependent on the heating rate and the amount of chemisorbed species. Additionally, the recovery of the initial loading state is described as a convergence to the unloaded reference. This description agrees fully with the interpretation of the results on $NO_x$ loaded $KMnO_4$/La-$Al_2O_3$ in Figure 11. However, applying eTPD, these electrical results were additionally verified by the analysis of the simultaneous desorption peak (Figure 9(a)). Yamazoe *et al.* [54] and Rodríguez-Gonzáles *et al.* [55] compared the conductivity with the evolution of desorbed gases as well, but these tests were performed on multiple samples in different setups. The Simon group [55–57] investigated the temperature dependent

$NH_3$ loading level of zeolites being active for the selective catalytic reduction (SCR) of $NO_x$. The conductivity upon heating reveals information on the conduction mechanism, the $NH_3$ desorption temperature as well as the SCR active temperature region allowing for *in-situ* reaction monitoring. Kubinski *et al.* [58] demonstrated that the average resistance during the thermally-induced $NH_3$ release from an SCR zeolite catalyst correlates with the former $NH_3$ exposure. This enables *in-situ* monitoring of the amount of sorbed $NH_3$ with a higher sensitivity compared to those in the $NH_3$ sorption mode [58].

The equivalency of the two conductivity-related sensor responses $\Delta R_{rel}$ and $F_G$ of $KMnO_4$/La-$Al_2O_3$ as a measure for the cumulated $NO_x$ exposure is demonstrated in Figure 13 as a monotone and almost linear correlation, independent of the type of exposed $NO_x$ species. Both values can be applied as $NO_x$ dosimeter-type sensor responses and correlate linearly with the quantity of sorbed $NO_x$, enabling *in-situ* monitoring of the loading state, although they are analyzed upon $NO_x$ sorption at 380 °C ($\Delta R_{rel}$) and upon $NO_x$ release by heating up to 650 °C ($F_G$), respectively. Hence, dependent on the application and the information of interest, two different sensing modes are feasible with the proposed impedimetric $NO_x$ dosimeter based on $KMnO_4$. In both cases, $NO_x$ is accumulated in the sensitive layer at sorption temperature and thermally released during periodic regeneration intervals. However, in the first method, the change in the conductance during $NO_x$ accumulation in the low loading state is monitored as a continuous and linear measure for the cumulated $NO_x$ exposure as well as for the amount of sorbed $NO_x$. Concentration information can be obtained time-continuously from the signal derivative. On the contrary, in the second method, the integrated difference between the conductivity during $NO_x$ release upon heating and the conductivity in the unloaded state serves as the measurand. Unfortunately, no time-continuous information on the $NO_x$ concentration can be obtained.

**Figure 13.** Correlation between electrical responses $\Delta R_{rel}$ (during sorption) and $F_G$ (upon regeneration) affected by $NO_x$ exposure.

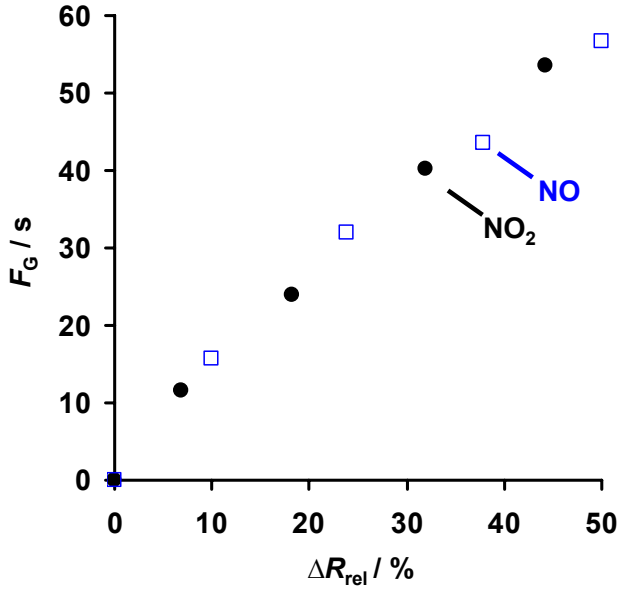


Simultaneous $NO_x$ detection in the sorption and release mode may be realized on one single sensor platform, with multiple independently heated sensitive layers, as described in [17]. A combination of both sensing modes to extract further information will be the focus of further research. The redundant

sensing information is expected to enable a plausibility consideration of the time resolved sensor signal during $NO_x$ sorption and of the regeneration success. Additionally, the linear measurement range for the $NO_x$ exposure is expected to be enhanced in the regeneration mode. Another important issue of gas sensors is the sensitivity to other gases as well as poisoning of sensitive layers, e.g., by $SO_2$ [59,60]. Since interfering gases might affect $NO_x$ sorption and release as well as the temperature-dependent conductivity differently, a combination of the electrical responses upon $NO_x$ sorption and release might be particularly useful.

## 5. Conclusions

This initial study demonstrates the suitability of decomposed $KMnO_4$ deposited on La-stabilized alumina as dosimeter-type sensitive material with two different operation methods and as a $NO_x$ sorbent in catalysts with electrical *in-situ* characterization potential. The impedimetric sensor response to low levels of NO and $NO_2$ was found to be irreversible under isothermal conditions at 380 °C. These dosimeter-type sensing characteristics are reproducible if sorbed $NO_x$ is released by heating up to 650 °C to recover the sorption capacity. The resistance change of $KMnO_4$/La-$Al_2O_3$ in the low loaded state correlates linearly with the cumulated $NO_x$ exposure, enabling low level $NO_x$ detection due to the $NO_x$ oxidizing and sorbing capability of the $KMnO_4$-based material. The sensor responds slightly more sensitively to NO than to $NO_2$.

By combining the electrical response with thermal programmed desorption (eTPD), the change in the electrical properties of $KMnO_4$/La-$Al_2O_3$ can be related to the thermally released quantity of $NO_x$. This novel method enables the quantitative correlation between the electrical response and the $NO_x$ loading in the sensor (or catalyst) material. The amount of $NO_x$ sorbed on $KMnO_4$/La-$Al_2O_3$, estimated from the released amount, increases linearly with the cumulated $NO_x$ exposure (or dose), resulting in a time constant $NO_x$ sorption rate. The resistance change during $NO_x$ sorption correlates linearly with the amount of sorbed $NO_x$ and hence with the $NO_x$ exposure. Therefore, information on the $NO_x$ concentration can be obtained time-continuously from the signal derivative. Additionally, the thermally activated conductivity of $KMnO_4$ is affected by the $NO_x$ release upon heating. The deviation from the course of the temperature-dependent conductivity in the unloaded state is another linear measure for the previously stored amount of $NO_x$. As a result, $NO_x$ exposure and $NO_x$ loading dependent electrical response can be analyzed either during $NO_x$ sorption or release enabling dosimeter-like $NO_x$ sensing or electrical *in-situ* monitoring.

## Acknowledgements

The authors gratefully acknowledge material preparation by Tina Weller, SEM analysis by Angelika Mergner (both of Lehrstuhl für Funktionsmaterialien), XRD analysis by Sandra Haupt and Wolfgang Milius (both of Lehrstuhl für Anorganische Chemie I, J. Breu) and the possibility to perform BET measurements at Lehrstuhl für Chemische Verfahrenstechnik (A. Jess). R.M. thanks the German Research Foundation (DFG) for supporting this work under grant number MO 1060/15-1 and under MO 1060/9-1 as part of the collaboration with H.L.T. H.L.T. thanks the Division of Materials Research, National Science Foundation under the Material World Network (DMR-0908627) as part of the

collaboration with R.M. This publication was funded by the German Research Foundation (DFG) and the University of Bayreuth in the funding program "Open Access Publishing".

## References

1. Fergus, J.W. Materials for high temperature electrochemical $NO_x$ gas sensors. *Sens. Actuators B Chem*. **2007**, *121*, 652–663.
2. Yamazoe, N.; Miura, N. Environmental gas sensing. *Sens. Actuators B Chem*. **1994**, *20*, 95–102.
3. Afzal, A.; Cioffi, N.; Sabbatini, L.; Torsi, L. $NO_x$ sensors based on semiconducting metal oxide nanostructures: Progress and perspectives. *Sens. Actuators B Chem*. **2012**, doi:10.1016/j.snb.2012.05.026.
4. Directive 2008/50/EC of the european parliament and of the council of 21 May 2008 on ambient air quality and cleaner air for europe. *Off. J. EU* **2008**, *L152/1*, 1–44.
5. Twigg, M.V. Progress and future challenges in controlling automotive exhaust gas emissions. *Appl. Catal. B* **2007**, *70*, 2–15.
6. Groß, A.; Beulertz, G.; Marr, I.; Kubinski, D.J.; Visser, J.H.; Moos, R. Dual mode $NO_x$ sensor: Measuring both the accumulated amount and instantaneous level at low concentrations. *Sensors* **2012**, *12*, 2831–2850.
7. Matsuguchi, M.; Kadowaki, Y.; Tanaka, M. A QCM-based $NO_2$ gas detector using morpholine-functional cross-linked copolymer coatings. *Sens. Actuators B Chem*. **2005**, *108*, 572–575.
8. Sasaki, D.Y.; Singh, S.; Cox, J.D.; Pohl, P.I. Fluorescence detection of nitrogen dioxide with perylene/PMMA thin films. *Sens. Actuators B Chem*. **2001**, *72*, 51–55.
9. Tanaka, T.; Guilleux, A.; Ohyama, T.; Maruo, Y.Y.; Hayashi, T. A ppb-level $NO_2$ gas sensor using coloration reactions in porous glass. *Sens. Actuators B Chem*. **1999**, *56*, 247–253.
10. Jung, W.; Sahner, K.; Leung, A.; Tuller, H.L. Acoustic wave-based $NO_2$ sensor: Ink-jet printed active layer. *Sens. Actuators B Chem*. **2009**, *141*, 485–490.
11. Geupel, A.; Schönauer, D.; Röder-Roith, U.; Kubinski, D.J.; Mulla, S.; Ballinger, T.H.; Chen, H.-Y.; Visser, J.H.; Moos, R. Integrating nitrogen oxide sensor: A novel concept for measuring low concentrations in the exhaust gas. *Sens. Actuators B Chem*. **2010**, *145*, 756–761.
12. Brunet, J.; Parra Garcia, V.; Pauly, A.; Varenne, C.; Lauron, B. An optimised gas sensor microsystem for accurate and real-time measurement of nitrogen dioxide at ppb level. *Sens. Actuators B Chem*. **2008**, *134*, 632–639.
13. Yamazoe, N.; Shimanoe, K. Overview of Gas Sensor Technology. In *Science and Technology of Chemiresistor Gas Sensors*; Aswal, D.K., Gupta, S.K., Eds.; Nova Science Publishers, Inc.: New York, NY, USA, 2007; pp. 1–31.
14. Shu, J.H.; Wikle, H.C.; Chin, B.A. Passive chemiresistor sensor based on iron (II) phthalocyanine thin films for monitoring of nitrogen dioxide. *Sens. Actuators B Chem*. **2010**, *148*, 498–503.
15. Groß, A.; Bishop, S.R.; Yang, D.J.; Tuller, H.L.; Moos, R. The electrical properties of $NO_x$-storing carbonates during $NO_x$ exposure. *Solid State Ionics* **2012**, *225*, 317–323.
16. Groß, A.; Richter, M.; Kubinski, D.J.; Visser, J.H.; Moos, R. The effect of the thickness of the sensitive layer on the performance of the accumulating $NO_x$ sensor. *Sensors* **2012**, *12*, 12329–12346.

17. Brandenburg, A.; Kita, J.; Groß, A.; Moos, R. Novel tube-type LTCC transducers with buried heaters and inner interdigitated electrodes as a platform for gas sensing at various high temperatures. *Sens. Actuators B Chem*. **2013**, doi:10.1016/j.snb.2012.12.119.
18. Geupel, A.; Kubinski, D.J.; Mulla, S.; Ballinger, T.H.; Chen, H.Y.; Visser, J.H.; Moos, R. Integrating $NO_x$ sensor for automotive exhausts—a novel concept. *Sens. Lett.* **2011**, *9*, 311–315.
19. Fruhberger, B.; Stirling, N.; Grillo, F.G.; Ma, S.; Ruthven, D.; Lad, R.J.; Frederick, B.G. Detection and quantification of nitric oxide in human breath using a semiconducting oxide based chemiresistive microsensor. *Sens. Actuators B Chem*. **2001**, *76*, 226–234.
20. Brogren, C.; Karlsson, H.T.; Bjerle, I. Absorption of NO in an alkaline solution of $KMnO_4$. *Chem. Eng. Technol.* **1997**, *20*, 396–402.
21. Wei, Z.-S.; Niu, H.-J.; Ji, Y.-F. Simultaneous removal of $SO_2$ and $NO_x$ by microwave with potassium permanganate over zeolite. *Fuel Process. Technol.* **2009**, *90*, 324–329.
22. Becerra, M.E.; Arias, N.P.; Giraldo, O.H.; López-Suárez, F.E.; Illán-Gómez, M.J.; Bueno-López, A. Soot combustion manganese catalysts prepared by thermal decomposition of $KMnO_4$. *Appl. Catal. B* **2011**, *102*, 260–266.
23. Lesage, T.; Saussey, J.; Malo, S.; Hervieu, M.; Hedouin, C.; Blanchard, G.; Daturi, M. Operando FTIR study of $NO_x$ storage over a $Pt/K/Mn/Al_2O_3$-$CeO_2$ catalyst. *Appl. Catal. B* **2007**, *72*, 166–177.
24. Becerra, M.-E.; Arias, N.-P.; Giraldo, O.-H.; López-Suárez, F.-E.; Illán-Gómez, M.-J.; Bueno-López, A. Alumina-supported manganese catalysts for soot combustion prepared by thermal decomposition of $KMnO_4$. *Catalysts* **2012**, *2*, 352–367.
25. Boldyrev, V.V. Mechanism of thermal decomposition of potassium permanganate in the solid phase. *J. Phys. Chem. Solids* **1969**, *30*, 1215–1223.
26. Boldyrev, V.V. Topochemistry of thermal decompositions of solids. *Thermochimica Acta* **1986**, *100*, 315–338.
27. Galwey, A.K.; Brown, M.E. An appreciation of the chemical approach of V. V. Boldyrev to the study of the decomposition of solids. *J. Therm. Anal. Calorim.* **2007**, *90*, 9–22.
28. Kabanov, A.A. The application of electrophysical effects to the study of the thermal decomposition of solids. *Russ. Chem. Rev.* **1971**, *40*, 953–963.
29. Rosseinsky, D.R.; Tonge, J.S. Electron transfer in solids. Temperature dependence of dielectric relaxation and conductivity in mixed-valence potassium manganate–permanganate. *J. Chem. Soc. Faraday Trans.* **1982**, *78*, 3595–3603.
30. Kappenstein, C.; Pirault-Roy, L.; Guérin, M.; Wahdan, T.; Ali, A.A.; Al-Sagheer, F.A.; Zaki, M.I. Monopropellant decomposition catalysts: V. Thermal decomposition and reduction of permanganates as models for the preparation of supported $MnO_x$ catalysts. *Appl. Catal. A* **2002**, *234*, 145–153.
31. Schönauer, D.; Moos, R. Detection of water droplets on exhaust gas sensors. *Sens. Actuators B Chem.* **2010**, *148*, 624–629.
32. Groß, A.; Weller, T.; Tuller, H.L.; Moos, R. Electrical conductivity study of $NO_x$ trap materials $BaCO_3$ and $K_2CO_3/La$-$Al_2O_3$ during $NO_x$ exposure. *Sens. Actuators B Chem.* **2013**, doi:10.1016/j.snb.2013.01.083.
33. Wu, X.; Lin, F.; Wang, L.; Weng, D.; Zhou, Z. Preparation methods and thermal stability of Ba-Mn-Ce oxide catalyst for $NO_x$-assisted soot oxidation. *J. Environ. Sci.* **2011**, *23*, 1205–1210.

34. Wu, X.; Liu, S. Lin, F.; Weng, D. Nitrate storage behavior of $Ba/MnO_x$-$CeO_2$ catalyst and its activity for soot oxidation with heat transfer limitations. *J. Hazard. Mater.* **2010**, *181*, 722–728.
35. Xiao, J.-H.; Li, X.-H.; Deng, S.; Xu, J.-C.; Wang, L.-F. The $NO_x$ oxidation-storage and tolerance of $SO_2$ poison of $Mn/Ba/Al_2O_3$ catalyst. *Acta Phys. Chim. Sin.* **2006**, *22*, 815–819.
36. Xiao, J.; Li, X.; Deng, S.; Wang, F.; Wang, L. $NO_x$ storage-reduction over combined catalyst $Mn/Ba/Al_2O_3$–$Pt/Ba/Al_2O_3$. *Catal. Commun.* **2008**, *9*, 563–567.
37. Beulertz, G.; Groß, A.; Moos, R.; Kubinski, D.J.; Visser, J.H. Determining the total amount of $NO_x$ in a gas stream – Advances in the accumulating gas sensor principle. *Sens. Actuators B Chem.* **2012**, *175*, 157–162.
38. Gill, L.J.; Blakeman, P.G.; Twigg, M.V.; Walker, A.P. The use of $NO_x$ adsorber catalysts on diesel engines. *Top. Catal.* **2004**, *28*, 157–164.
39. Roy, S.; Baiker, A. $NO_x$ storage-reduction catalysis: From mechanism and materials properties to storage-reduction performance. *Chem. Rev.* **2009**, *109*, 4054–4091.
40. Epling, W.S.; Campbell, L.E.; Yezerets, A.; Currier, N.W.; Parks, J.E., II. Overview of the fundamental reactions and degradation mechanism of $NO_x$ storage/reduction catalysts. *Catal. Rev. Sci. Eng.* **2004**, *46*, 163–245.
41. Fremerey, P.; Reiß, S.; Geupel, A.; Fischerauer, G.; Moos, R. Determination of the $NO_x$ loading of an automotive lean $NO_x$ trap by directly monitoring the electrical properties of the catalyst material itself. *Sensors* **2011**, *11*, 8261–8280.
42. Moos, R.; Zimmermann, C.; Birkhofer, T.; Knezevic, A.; Plog, C.; Busch, M.R.; Ried, T. Sensor for Directly Determining the State of a $NO_x$ Storage Catalyst. In Proceedings of the SAE World Congress and Exhibition, Detroit, MI, USA, 14–17 April 2008; doi:10.4271/2008-01-0447.
43. Moos, R.; Wedemann, M.; Spörl, M.; Reiß, S.; Fischerauer, G. Direct catalyst monitoring by electrical means: An overview on promising novel principles. *Top. Catal.* **2009**, *52*, 2035–2040.
44. Le Phuc, N.; Courtois, X.; Can, F.; Royer, S.; Marecot, P.; Duprez, D. $NO_x$ removal efficiency and ammonia selectivity during the $NO_x$ storage-reduction process over $Pt/BaO(Fe, Mn, Ce)/Al_2O_3$ model catalysts. Part I: Influence of Fe and Mn addition. *Appl. Catal. B* **2011**, *102*, 353–361.
45. Bentrup, U.; Brückner, A.; Richter, M.; Fricke, R. $NO_x$ adsorption on $MnO_2$/NaY composite: An *in situ* FTIR and EPR study. *Appl. Catal. B* **2001**, *32*, 229–241.
46. Fricke, R.; Schreier, E.; Eckelt, R.; Richter, M.; Trunschke, A. Non-isothermal $NO_x$ storage/release over manganese based traps: Mechanistic considerations. *Top. Catal.* **2004**, *30/31*, 193–198.
47. Kijlstra, W.S.; Brands, D.S.; Poels, E.K.; Bliek, A. Mechanism of the selective catalytic reduction of NO by $NH_3$ over $MnOx/Al_2O_3$. *J. Catal.* **1997**, *171*, 208–218.
48. Li, W.B.; Yang, X.F.; Chen, L.F.; Wang, J.A. Adsorption/desorption of $NO_x$ on $MnO_2/ZrO_2$ oxides prepared in reverse microemulsions. *Catal. Today* **2009**, *148*, 75–80.
49. Takeuchi, M.; Matsumoto, S. $NO_x$ storage-reduction catalysts for gasoline engines. *Top. Catal.* **2004**, *28*, 151–156.
50. Colin, Y.; Fortin, B.; Raoult, F. Resistance variation of a semiconduction thin film during a thermal desorption. *Phys. Status Solidi A* **1981**, *67*, 485–495.
51. Fortin, B.; Larzul, H.; Lebigot, J.; Raoult, F.; Rosse, G. Model for the resistance variation of a thin semiconducting film during temperature- programmed desorption: Application to the $O_2$-CdSe system. *Thin Solid Films* **1985**, *131*, 51–68.

52. Sanjines, R.; Lévy, F.; Demarne, V.; Grisel, A. Some aspects of the interaction of oxygen with polycrystalline $SnO_x$ thin films. *Sens. Actuators B Chem*. **1990**, *1*, 176–182.
53. Rossé, G.; Raoult, F.; Fortin, B. Regeneration of CdSe thin films after oxygen chemisorption. *Thin Solid Films* **1984**, *111*, 175–181.
54. Yamazoe, N.; Fuchigami, J.; Kishikawa, M.; Seiyama, T. Interactions of tin oxide surface with $O_2$, $H_2O$ and $H_2$. *Surf. Sci.* **1979**, *86*, 335–344.
55. Rodríguez-González, L.; Rodríguez-Castellón, E.; Jiménez-López, A.; Simon, U. Correlation of TPD and impedance measurements on the desorption of $NH_3$ from zeolite H-ZSM-5. *Solid State Ionics* **2008**, *179*, 1968–1973.
56. Simons, T.; Simon, U. Zeolites as nanoporous, gas-sensitive materials for *in situ* monitoring of $DeNO_x$-SCR. *Beilstein J. Nanotechnol.* **2012**, *3*, 667–673.
57. Simons, T.; Simon, U. Zeolite H-ZSM-5: A Microporous Proton Conductor for the *in situ* Monitoring of $DeNO_x$-SCR. *Mater. Res. Soc. Symp. Proc.* **2011**, doi:10.1557/opl.2011.1337.
58. Kubinski, D.J.; Visser, J.H. Sensor and method for determining the ammonia loading of a zeolite SCR catalyst. *Sens. Actuators B Chem*. **2008**, *130*, 425–429.
59. Groß, A.; Hanft, D.; Beulertz, G.; Marr, I.; Kubinski, D.J.; Visser, J.H.; Moos, R. The effect of $SO_2$ on the sensitive layer of a $NO_x$ dosimeter. *Sens. Actuators B Chem*. **2012**, doi:10.1016/j.snb.2012.10.039.
60. Rettig, F.; Moos, R.; Plog, C. Sulfur adsorber for thick-film exhaust gas sensors. *Sens. Actuators B Chem*. **2003**, *93*, 36–42.